Controlled Experiments and Optimized Theory of Absorption Spectra of Li Metal and Salts

Subhayan Roychoudhury§#‡, Zengqing Zhuo§‡, Ruimin Qiao§‡, Liwen Wan¶, Yufeng Liang#, Feng Pan†, Yi-de Chuang§*, David Prendergast#* and Wanli Yang§*

§Advanced Light Source, Lawrence Berkeley National Laboratory, 1 Cyclotron Road, Berkeley CA 94720, USA

¶Lawrence Livermore National Laboratory, 7000 East Avenue, Livermore, California 94550, USA

†School of Advanced Materials, Peking University Shenzhen Graduate School, Shenzhen 518055, China

#The Molecular Foundry, Lawrence Berkeley National Laboratory, 1 Cyclotron Road, Berkeley CA 94720, USA

KEYWORDS: X-ray absorption spectroscopy, Theory of spectroscopy, Lithium Metal, Lithium salts, Battery chemistry, Li-K spectroscopy

ABSTRACT: Investigations of Li metal and ionic compounds through experimental and theoretical spectroscopy has been of tremendous interest due to their prospective applications in Li-metal and Li-ion batteries. Li *K*-edge soft X-ray absorption spectroscopy (sXAS) provides the most direct spectroscopic characterization; unfortunately, due to the low core-level energy and the highly reactive surface, Li-*K* sXAS of Li metal has been extremely challenging, as evidenced by many controversial reports. Here, through controlled and ultra-high energy resolution experiments of two kinds of *in-situ* prepared samples, we report the intrinsic Li-*K* sXAS of Li-metal that displays a prominent leading peak that has never been revealed before. Furthermore, theoretical simulations show that, due to the low number of valence electrons in Li, the Li-*K* sXAS is strongly affected by the response of the valence electrons to the core-hole. We successfully reproduce the Li-*K* sXAS by state-of-the-art calculations with considerations of a number of relevant parameters such as temperature, resolution, and especially, contributions from transitions which are forbidden in the single-particle treatment. Such a comparative experimental and theoretical investigation is further extended to a series of Li ionic compounds, which highlight the importance of considering the total and single-particle energies for obtaining an accurate alignment of the spectra. Our work provides the first reliable Li-*K* sXAS of Li metal surface with advanced theoretical calculations. The experimental and theoretical results provide a critical benchmark for studying Li chemistry in both metallic and ionic states.

INTRODUCTION:

Lithium-based electrochemical devices for energy storage, i.e., batteries, have been ubiquitous in modern life since their commercialization in the early 1990s[1]. However, in spite of several decades of extensive efforts, the holy grail of a high-energy-density lithium battery based on a Li metal anode is yet to be achieved. The challenge of utilizing Li metal electrodes remains formidable in both practical optimization and fundamental understanding[2,3]. Additionally, the electrolyte and its associated solid-electrolyte interphase (SEI) and cathode-electrolyte interphase (CEI) remain the least understood functional components despite being critical to battery performance[4,5]. Fundamentally, many limiting factors in battery operation are associated with Li-ion diffusion, which is extremely difficult to track due to the lack of techniques that could directly and precisely follow the Lithium chemistry. Therefore, a direct probe of Li in its metallic and ionic states with elemental and chemical sensitivities becomes crucial.

The technical challenges for a direct probe of Li chemistry stem from many intrinsic characters. First, as an alkali metal, Li metal is highly reactive, so its surface is unstable under ambient environment. As revealed by our controlled experiments below, even in ultra-high vacuum environment, the chemical state of the surface of Li metal could still evolve quickly in minutes, not to mention the typical Ar glove box environment with much higher level of reactive gas residuals. Second, as a popular technique, soft X-ray absorption spectroscopy (sXAS) has long been employed to study battery materials for many other elements, especially through its photon-in-photon-out (PIPO) mode with relative bulk sensitivity[6]. However, the only core-level excitation of Li, the *K*-edge electron excitation from *1s* to *2p*, falls into a very low energy range, from 55 to 65 eV. This low energy naturally leads to a shallow probe depth (attenuation length ~50nm, thus probe depth ~25 nm) even in the sXAS PIPO mode[7]. Third, for ionic compounds, it has been observed that soft X-rays around the Li-*K* edge could introduce radiation damage effects[8]. So, experiments with controlled surface preparation and irradiation are both critical for obtaining reliable data. Fourth, due to these technical challenges, compared with a large number of sXAS reports of other elements, e.g., O and transition metals, there is only a handful of literature with experimental results of Li-*K* sXAS[8–16]. Additionally, due to the lack of benchmark and fundamental understandings of Li-*K* spectra,

Li-*K* sXAS, in spite of being the most direct spectroscopic probe of Li, was typically utilized as just a supplementary indication of the amount of Li during the lithiation/delithiation process[16]. Even worse, the reported spectra of Li metal have varied significantly between different reports, and all Li-*K* XAS reports of Li metal contradict the findings by other techniques such as electron energy loss spectroscopy (EELS) and hard X-ray Raman Spectroscopy (XRS)[9–11,17–19].

Theoretically, Li-K sXAS of various ionic compounds has been computed[20,21] with the help of Kohn-Sham (KS) Density Functional Theory (DFT)[22,23] and many-body perturbation theory[24,25]. Researchers also simulated Li-*K* sXAS of metallic Li using wavefunction based single particle techniques and perturbative treatments[19,26]. However, the precision and validity of the theoretical calculations suffer the lack of reliable experimental results, so it has been hard to achieve a quantitative level of comparison between the theory and experiment. Therefore, establishing a benchmark of reliable experimental data and developing theoretical calculations of Li-*K* are equally important towards the direct probe of Li chemistry.

In this paper, controlled experiments were carried out by employing two kinds of *in-situ* Lithium metal sample preparations, evaporation and cleaving, directly in ultra-high vacuum (UHV) with ultra-high experimental resolution (0.01 eV experimental resolution). Aging and radiation effects are tested separately. We show that the surface of Li metal is highly reactive, even in 1.4×10^{-10} Torr UHV environment, evolving into a spectrally dominant Li_2O layer. Samples prepared by *in-situ* Li evaporation in UHV display the degradation signature right after preparation, likely due to the immediate reaction at the high temperature of the evaporation process. Comparative experiments on three sets of samples show that the surface prepared through *in-situ* cleaving finally rules out all degradation possibilities, and allows the collection of the intrinsic Li-*K* spectrum of Li metal. Li-*K* sXAS of Li metal displays a prominent leading peak at the absorption edge that has never been found before in any Li-*K* techniques including sXAS, EELS and XRS. Our theoretical calculations show that, due to the low atomic number of Li, the poorly screened core-hole strongly affects the unoccupied orbitals. An accurate calculation requires the explicit consideration of the orbital relaxation of all the valence electrons in response to the core-hole creation, which we simulate with the Many-body X-ray Absorption Spectroscopy (MBXAS) method[27–29]. We successfully explore the effects of finite temperature, spectral resolution, and contributions from transitions which are forbidden within a simplified single-particle framework, thereby achieving a successful reproduction of the experimental data and explain the previous controversial reports. We further investigate a series of Li ionic compounds based on the same theoretical approach. The simulations show that accurate spectral alignment among different compounds can be obtained if each calculated spectrum is rigidly shifted by a term containing total energies as well as single-particle KS energies computed using a hybrid-exact-exchange functional. Our work provides the first reliable dataset of Li-*K* sXAS of Li metal through carefully controlled experiments, indicates the possible sources of contradictions among the previous reports, and establishes the framework for optimized theoretical calculations to obtain a simulation of Li-*K* sXAS spectroscopy with quantitative accuracy in terms of spectral lineshape and alignment.

EXPERIMENTAL AND THEORETICAL SECTION

Li-*K* sXAS was performed at the ultra-high energy resolution Beamline 4.0.3 (MERLIN) of the Advanced Light Source at Lawrence Berkeley National Laboratory. The beamline covers energies ranging from 10 eV to ~150 eV, which is ideal for Li *K*-edge, with a photon flux of 10^{11}/sec. The experimental energy resolution is better than 10 meV. Due to such a high instrumental resolution, it is expected that the finite peak width of the spectrum is predominantly a consequence of the thermal effects and the finite lifetimes of the Li quasiparticle orbitals, including the core-hole and the conduction orbitals. Both total fluorescence yield (TFY) and the total electron yield (TEY) signals are collected; however, we note that due to the very low photon energy of Li-*K* around 50-60 eV, the attenuation of the X-ray photons is around 50 nm [Supplementary FIG.S5], so even for the TFY collected in the reflection mode (photon-in-photon-out), the majority of the signals are from the surface ~20 nm, roughly at the same scale as the typical probe depth (~10 nm) of TEY that is dominated by secondary electrons[30]. This is confirmed by the similar Li-*K* TEY and TFY lineshape of the Li-metal samples, as shown below. For Li salts, due to their highly insulating property, TEY suffers electrostatic charging upon irradiation, so we focus on TFY signals in this work.

Two different *in-situ* sample preparation methods are used to prepare the Li metal samples: cleaving a thick piece of Li metal and Li evaporation. The *in-situ* cleaving of the Li metal surface was done by installing a cleaned blade through a motion feedthrough into the UHV (1.4×10^{-10} Torr) chamber, which is used to cut/scratch through the soft Li metal to expose a fresh surface. Evaporated Li metal surfaces are prepared by supplying a controlled current through a SAES Li metal dispenser, which has been well degassed before the Li evaporation. We note that SAES alkali metal dispensers are typical alkali metal sources in scientific studies for controlled Alkali-metal evaporation in UHV[31]. Surprisingly, the two kinds of *in-situ* prepared samples display clear spectral differences (**FIG. 1 & 2**), which indicate the high reactivity of the Li metal surface even in 10^{-10} Torr ultra-high vacuum (UHV) and provide the chance to clarify the discrepancies among previous reports.

On the theory front, we simulate the spectra with the MBXAS formalism which approximates the initial (final) state as a Slater determinant composed of two distinct sets of valence KS orbitals obtained in the absence (presence) of a core-hole. As discussed in the next section, with such explicit consideration of the relaxation of valence electrons, MBXAS is able to show that electronic transitions which are forbidden in the conventional single-particle approach can actually have significant amplitude. For simulating room temperature effects, we use MBXAS in conjunction with ab-initio molecular dynamics (MD) which leads to an overall smoothening of the spectrum, in accordance with the experimental results. Finally, in order to obtain an accurate alignment among the spectra of different materials, we propose a scheme based on a combined consideration of the total and single-particle energies obtained using a non-local hybrid-exact-exchange functional.

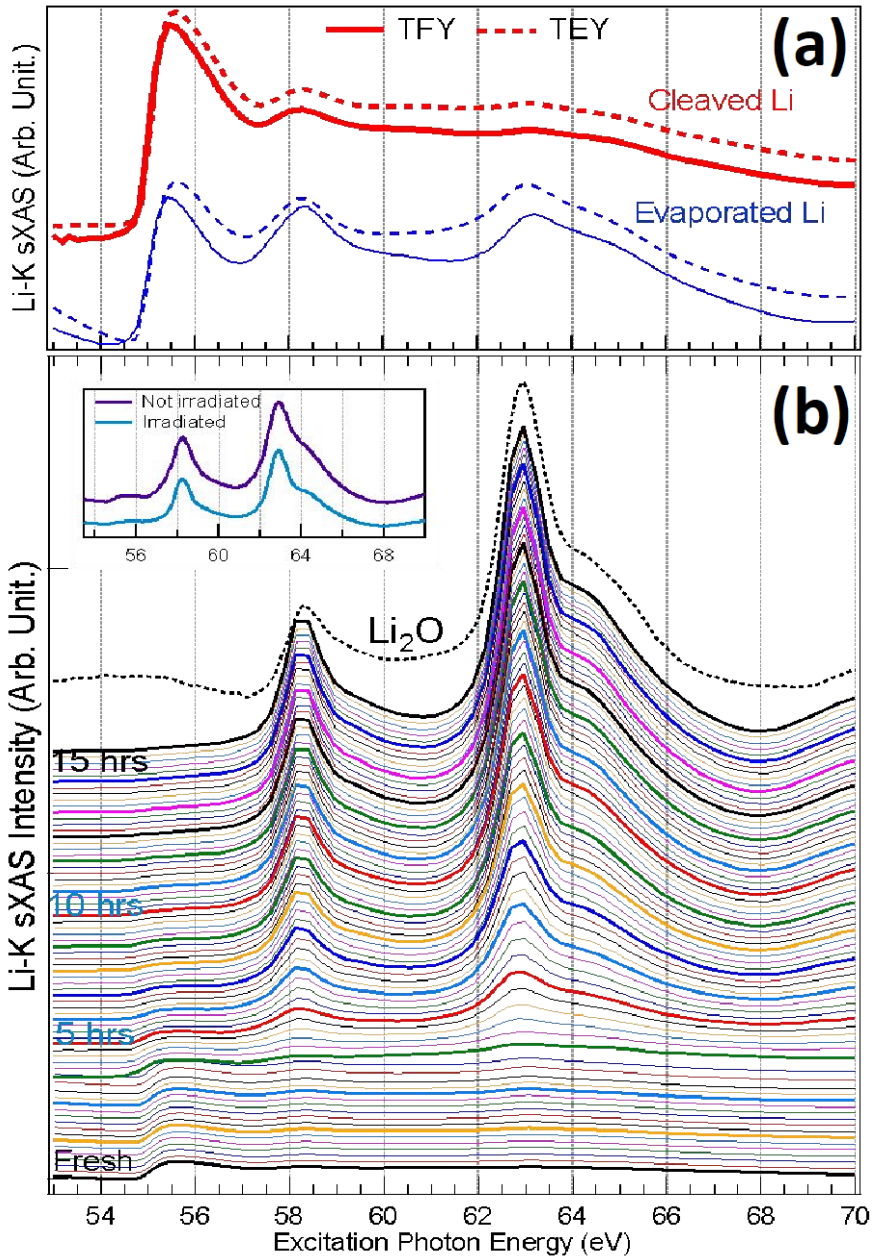

FIG. 1 Soft x-ray Li-*K* sXAS collected on lithium metal surfaces prepared *in-situ* in two different ways. (a) The red and the blue spectra show the Li K-edge of metallic Li prepared by in-situ cleaving and evaporation, respectively. (b) The spectral evolution of a freshly cleaved Li metal surface (bottom spectrum), then every 10 minutes in UHV of 1.4×10^{-10} Torr. The 15 thick spectra indicate the lineshape evolution every one hour. Features from Li_2O emerges after only 20 minutes in HUV and dominate the degraded spectral lineshape. The red spectrum in panel (a) is an amplified view of the bottom spectrum in panel (b). Inset shows spectra collected on two spots with and without x-ray exposure during the 5 hours decay period in UHV. The lineshape degrades in the same way with only small quantitative differences, indicating that the lineshape decay is from surface aging, not irradiation effect.

RESULTS AND DISCUSSIONS

Li-*K* spectroscopy of Li metal: **FIG.1(a)** shows the K-edge absorption spectra, collected in both the TFY and TEY modes, of Li metal samples immediately after the preparation through *in-situ* cleaving (red), and *in-situ* evaporation (blue). The *in-situ* cleaved sample displays a striking leading peak. Such a dominating peak was not observed in previous Li-*K* sXAS reports at all[10,11] , and previous reports based on relatively bulk-sensitive techniques found a much weaker feature here[11,17,26,32]. This leading peak is also much suppressed in the evaporated-Li spectra with enhanced features at high energies. As plotted in **FIG.1(b)** with the dashed line on top, these high energy features match the Li_2O peaks, indicating that the sample surface already degraded right after the *in-situ* evaporation of Li-metal.

To investigate the Li-metal degradation even in ultra-high vacuum and to confirm that the spectra collected from the *in-situ* cleaved Li metal are intrinsic Li-metal signals, **FIG.1(b)** displays the sXAS recorded right after the cleaved metal surface is ex-

posed at a regular interval of 10 minutes each for 15 hours. The bottommost spectrum is from the freshly prepared sample, the same as the spectrum amplified in **FIG. 1(a)**. Moving from the bottom to the top, the 15 thick spectra indicate the lineshape evolution every one hour. Obvious change is observed after 20 minutes, when the profound 55.6 eV feature begins to diminish and the features at 58.4 eV and 62.9 eV start intensifying. The latter two resemble the peaks of the Li_2O spectrum, as shown by the reference spectra on top. After about 4 hours in the UHV chamber, evident features from Li_2O start to dominate the spectrum and the signatures of the freshly prepared Li sample are obscured. The results here clearly show that, even at 10^{-10} Torr UHV, the Li metal surface still degrades quickly. This naturally explains why experiments with Li metal samples loaded from Ar bags, or even in air, reported very different results[9,10]. Furthermore, the formation of Li_2O is intriguing, because O_2 molecules are removed in the UHV environment, and residual gas molecules of UHV at 10^{-10} Torr scale are mostly water and others with light molecular weight. The dominating Li_2O signals as the degradation product of Li metal under UHV implies a multi-step process instead of a direct Li oxidation with O_2 gas.

In order to rule out irradiation effects for such a spectral evolution, we collect the *in-situ* spectrum of a separate sample, prepared and stored under similar conditions in the UHV for 5 hours without any exposure to the X-ray beam. As shown in the inset of **FIG.1(b)**, this spectrum is essentially identical to that collected after 5 hours from the sample which has been exposed to X-rays. This supports our inference that the disappearance of the 55.6 eV peak with time is due to surface degradation even under UHV, not due to irradiation.

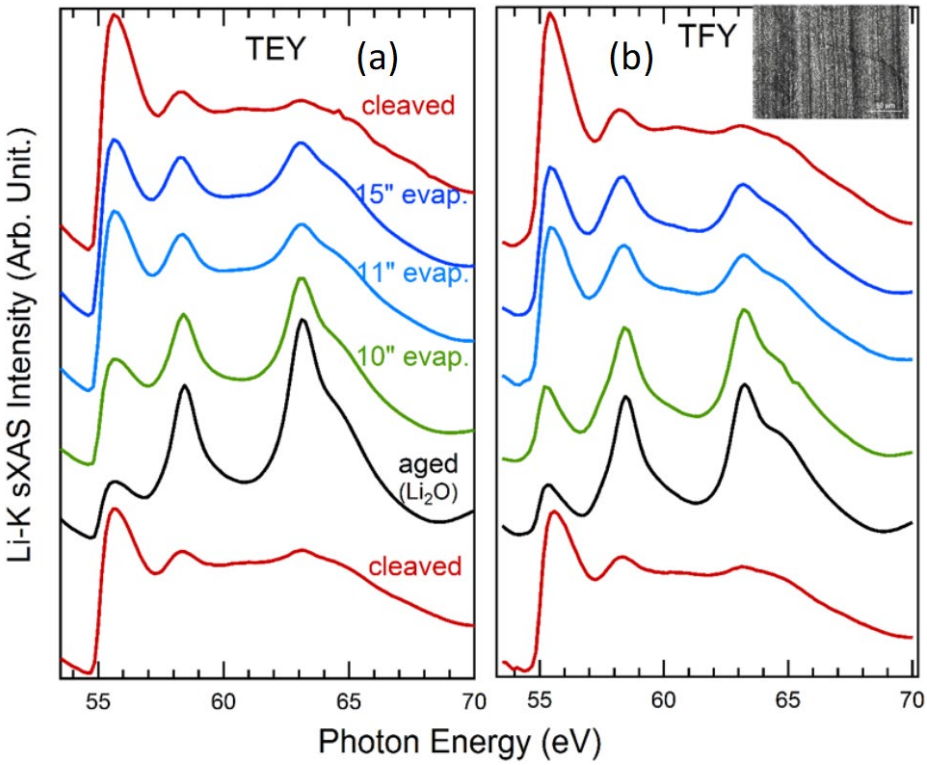

FIG. 2 Li-K sXAS TEY (a) and TFY (b) spectra collected on Lithium metal prepared in the sequence of i) *in-situ* cleaving (bottom, red), ii) in-vacuum aged (black), iii) Lithium evaporation for 10 (green), 11 and 15 (blue) minutes, and iv) another *in-situ* cleaving (top, red). Further lithium evaporation does not affect the overall spectral lineshape above 11 minutes. But the *in-situ* cleaving is a robust method for highly reproducible Li-*K* sXAS data. Inset shows the optical image of a cleaved surface after a blade scratching.

To conclude our study of the intrinsic Li-*K* sXAS of Li metal, we further tested samples prepared *in-situ* by both cleaving and evaporation on exactly the same piece of Li metal, as shown in **FIG.2** with the sample preparation sequence from the bottom to the top. First the cleaved Li metal sample displays the strong 55.6 eV leading peak, as found above. Second, the sample is left in UHV for about 3 hours, which displays the clear signature of the degradation product of Li_2O. Third, we evaporate lithium onto the surface of the sample with the evaporation time of 10, 11 and 15 minutes. The intensity of the Li_2O features show that the surface is getting cleaner with evaporation times up to 10 minutes, but further lithium evaporation longer than 11 minutes does not improve the overall spectral lineshape. Fourth, the red spectrum on top was collected on the same sample but with the surface cleaved again with the blade.

Therefore, these three sets of controlled experiments consistently suggest that the Li metal surface is highly reactive even under UHV conditions, which has led to the disappearance of the strong leading peak in previous Li metal sXAS studies. Because *in-situ* evaporation introduces a much higher local temperature around the sample, it is not surprising that a large amount of freshly evaporated Li degrades right after the deposition. Therefore, intrinsic Li metal *K*-edge sXAS could only be obtained within a short time after *in-situ* cleaving of the sample under UHV conditions. More importantly, the *in-situ* cleaved samples have displayed a very

robust and reproducible strong 55.6 eV peak that has not been found before even with bulk-sensitive techniques[18,19,26]. It is thus critical to interpret and validate this as the intrinsic Li-metal Li-*K* lineshape, and to understand the discrepancy between the Li-*K* sXAS here and other *K*-edge spectroscopic results.

Theoretical calculations of Li-*K* sXAS of Li metal

In order to reproduce and understand the striking lineshape of the intrinsic Li metal Li-*K* spectrum, we have explored different parameters and successfully developed the theoretical calculation of the Li K-edge sXAS based on DFT. Details of the computational parameters are presented in the Supplementary Information. The dipole transition matrix element for electronic excitation from an initial state $|\Psi_i\rangle$ to a final state $|\Psi_f\rangle$ is given by $\langle\Psi_f|\hat{\boldsymbol{O}}|\Psi_i\rangle$ where, $\hat{\boldsymbol{O}}$ is the many-electron dipole transition operator. In the single-particle *initial state* approximation, one approximates this term by

$$\langle\Psi_f|\hat{\boldsymbol{O}}|\Psi_i\rangle \approx S\,\langle\phi_c|\hat{o}|\phi_{core}\rangle, \qquad \textit{Eq. 1}$$

where ϕ_{core} is the single-particle wave-function of the core electron, ϕ_c is a Kohn-Sham (KS) unoccupied (i.e., conduction band) orbital obtained with the initial (ground) state DFT calculation in the absence of the core-hole, $\hat{o}$ is now the single-particle dipole transition operator, and S is a constant.

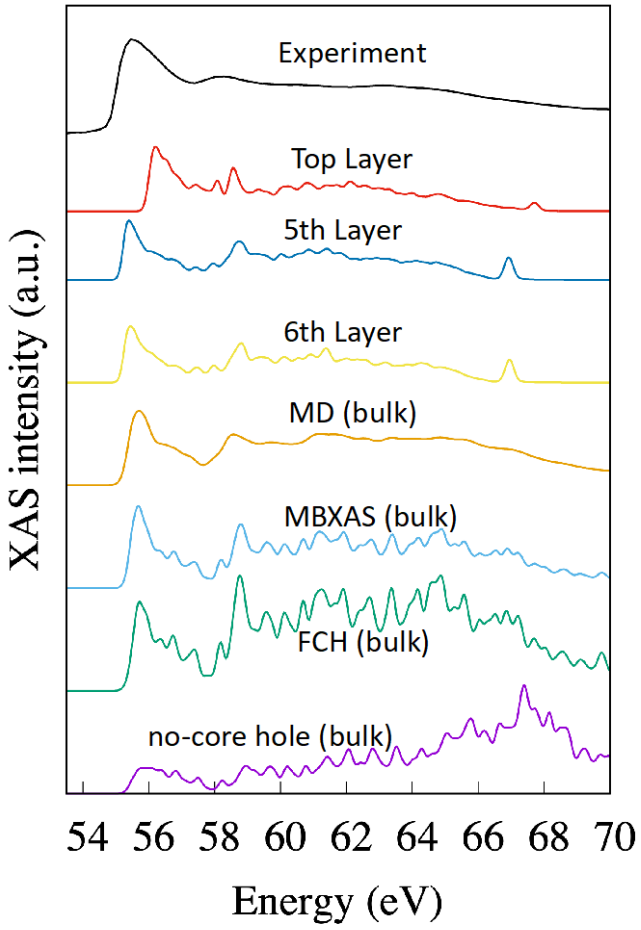

FIG. 3 Plot showing X-ray absorption spectra of Li metal. From top to bottom: Experimental spectrum, simulated (with MBXAS) spectrum of the top layer of a 12-layer Li slab, spectrum of the 5th layer of the same slab, spectrum of the 6th layer of the slab, MBXAS spectrum of bulk Li crystal obtained from a MD snapshot sampled at 300 K temperature, MBXAS spectrum of the static bulk Li crystal, spectrum of bulk Li computed with the FCH treatment, spectrum of bulk Li simulated in absence of the core-hole. A broadening of 0.1 eV has been applied to all the simulated spectra.

The simulation of the Li K-edge spectrum of bulk Li metal using this treatment is presented at the bottom of **FIG.3**. The *final state* Full Core-hole (*FCH*) spectrum, where ϕ_c in Eq. 1 is replaced by $\tilde{\phi}_c$, a final-state conduction orbital evaluated in presence of the core-hole, is shown above it in the same figure. The stark difference between the *initial-state* and the *FCH* spectra stems from the fact that, due to the low number of valence electrons in Li, the core-hole is poorly screened and consequently the unoccupied orbitals obtained in presence and absence of the core-hole are very different. In fact, the presence of the core-hole generates a set of localized orbitals trapped in the electrostatic potential of the excited core, which have significant overlap with the core orbital and result in higher intensity transitions in the spectrum.

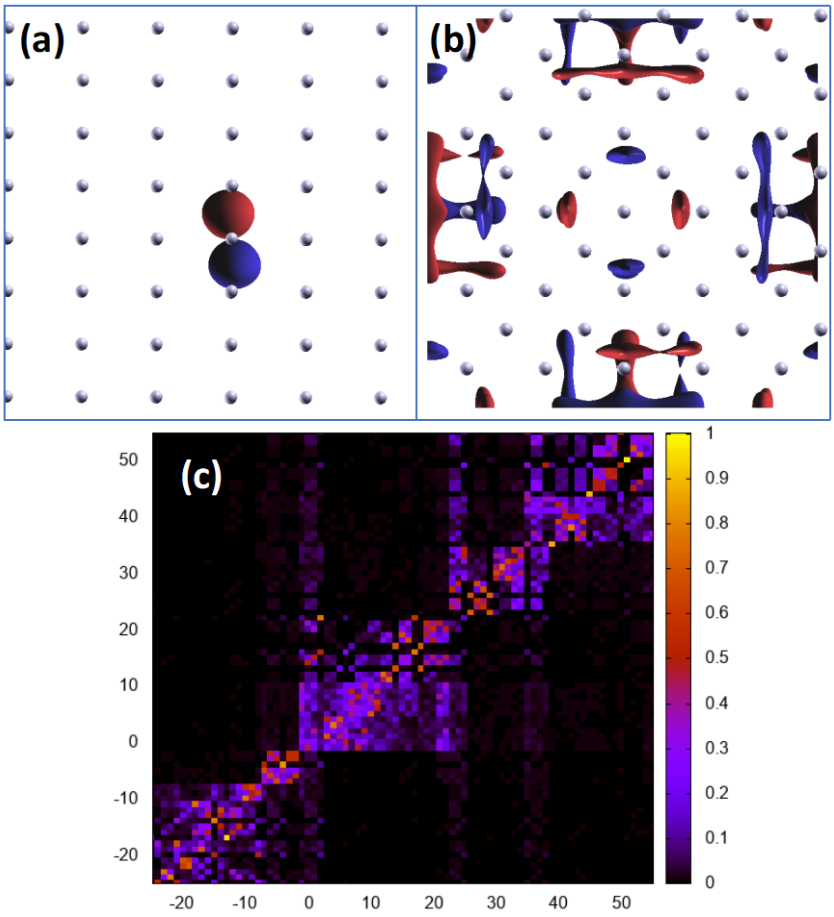

FIG. 4 Panels (a) and (b) show the isovalue plots of two unoccupied final state orbitals, transitions to which generate, according to the MBXAS treatment, two core-excitations having appreciable probability and contributing to the high-intensity peak in the Li-metal spectrum. Panel (a), shows a p-type orbital around the core-excited atom and consequently, such a transition is dominant in the FCH approach as well. However, the orbital in panel (b) has no presence on the core-excited (central) atom and thus the FCH calculation shows negligible probability for this transition. However, within the MBXAS treatment, both of the transitions correspond to appreciable probability. Panel (c) shows, within a certain range encompassing the highest occupied level, the absolute value of the overlap between the initial and the final state orbitals for the Γ point. The orbital with index = 1 is the lowest unoccupied level. As discussed in the main text (see the paragraph following Eq. 2), due to the presence of off-diagonal elements in this overlap matrix, it is possible that transitions which are forbidden in the single-particle FCH treatment have appreciable intensity in the MBXAS formalism.

The blue spectrum labeled "MBXAS (bulk)" is obtained with the recently developed MBXAS method, which calculates the matrix element $\langle \Psi_f | \widehat{\boldsymbol{O}} | \Psi_i \rangle$ by approximating the many-body wavefunction Ψ_f (Ψ_i) by a Slater determinant composed of KS orbitals computed in presence (absence) of the core-hole. Unlike the FCH spectrum, the MBXAS spectrum replicates a key feature of the experimental plot: the intensity of the first narrow peak is higher than that of the broad region at higher energy. Many of the low-energy near-edge transitions which have negligible probability in the single-particle treatment, have appreciable probability in the MBXAS treatment. **FIG.4 (a), (b)** show the isovalue plots of two unoccupied KS orbitals, transitions to which contribute significantly to the first peak intensity in MBXAS. While the orbital in panel (a) is a p-type orbital centered on the core-excited atom, and is therefore representative of a standard dipole-allowed transition in the FCH treatment, the orbital in panel (b) has negligible spatial overlap with the core-excited atoms and consequently, the associated single-particle excitation does not have any significant FCH transition-probability. However, the latter excitation has a substantial probability in the MBXAS method, which computes the transition matrix element as

$$\langle \Psi_f | \widehat{\boldsymbol{O}} | \Psi_i \rangle = \sum_{c}^{empty} \langle \Psi_f | \Psi_i^c \rangle \langle \phi_c | \hat{o} | \phi_{core} \rangle, \qquad \textit{Eq. 2}$$

where $|\Psi_i^c\rangle$ represents an excited state (with the core-orbital excited to the conduction orbital c) constructed with initial-state orbitals, which is represented by a Slater determinant composed of the valence occupied initial-state KS orbitals along with ϕ_c. The term $\langle \Psi_f | \Psi_i^c \rangle$, a matrix element between two Slater determinants built from orbitals of different self-consistent fields (final and ini-

tial state), can be re-expressed as the complex conjugate of a determinant composed of the overlap matrix elements between the final and initial state orbitals (See Supplementary Information for more details). A heat map showing the absolute values of such orbital overlaps is shown in **FIG.4(c)**. The presence of significant off-diagonal elements in this overlap matrix indicates the possibility that even if, for a certain final state orbital $\widetilde{\phi_{c\prime}}$, the transition-probability $\langle\widetilde{\phi_{c\prime}}|\hat{\mathbf{o}}|\phi_{\text{core}}\rangle$ is zero (i.e., the transition is dipole-forbidden in the FCH picture), it is possible that for a finite number of unoccupied initial-state orbitals ϕ_c, both of the terms $\langle\phi_c|\hat{\mathbf{o}}|\phi_{\text{core}}\rangle$ and $\langle\Psi_{\text{f}}|\Psi_i^c\rangle$ have non-zero contributions leading to an appreciable transition probability given by the sum in Eq.2 (Note that Ψ_{f} is given by a Slater determinant of which $\widetilde{\phi_{c\prime}}$ is a constituent orbital). The capability of including all these transition probabilities in our MBXAS calculations directly leads to the improved agreement with our experimental data on the strong 55.6 eV peak intensity beyond single-particle approximations.

In addition to the greater intensity of the first peak provided by the MBXAS theoretical approximation, we also note that there can be more mundane origins for a difference in relative intensity of the peaks. If, instead of a Gaussian broadening of 0.1 eV, we use a much higher broadening of 0.6 eV, the relative intensity of the higher energy region of the MBXAS spectrum turns out to exceed that of the first peak (see Supplementary Information). Therefore, in addition to surface aging reactions, a lower instrumental resolution can result in an experimental spectrum with relatively lower first peak intensity. This naturally explains the quantitative difference between the high resolution (10 meV experimental resolution) Li-*K* sXAS revealed here and the previous reports of hXRS and EELS results[18,19,25].

In order to obtain a more realistic simulation of the experiment, which is performed at room temperature, we run a first-principles MD simulation on a 128 atom lithium crystal supercell at 300 K temperature and calculate, using the MBXAS method, the average sXAS spectrum on a sample snapshot (see previous examples in Ref. [20]). The spectrum so obtained is labeled as "MD (bulk)" in **FIG.3**. Comparing this with the "MBXAS(bulk)" spectrum obtained at zero temperature, we can see that the thermal motion of the ions is responsible for the relative smoothness of the former spectrum at higher energies. In order to check for possible effects of surface layers on the spectrum, we run MBXAS simulations on a 12-layer (18.85 Å) thick slab of Li atoms. In **FIG.3**, we have shown the computed spectra corresponding to the top layer, the 5$^{\text{th}}$ layer and the 6$^{\text{th}}$ (middle) layer of the Li slab. MBXAS spectra for the 5$^{\text{th}}$ and the 6$^{\text{th}}$ layer of the slab look almost identical, indicating convergence. The spectra of these layers also replicate the crucial experimental observation that the narrow first peak has higher intensity than the high energy region. It is worth noting that the top layer spectrum blue shift to higher energies (~0.8 eV) due to the slightly lower electron population (i.e., oxidation) of the surface, undercoordinated Li atoms. A lower ground-state valence Lowdin population (0.8524) on a surface atom compared to one in the middle of the slab (0.9797) results in a higher binding energy for the core electron in the former. From **FIG.3** and **FIG.S3**, we conclude that only the spectrum of the topmost undercoordinated layer bears any significant difference with the bulk spectrum and that, in terms of the position and intensity of the first peak, the bulk limit is attained to an appreciable extent from the 2$^{\text{nd}}$ layer onward. A linear combination of the layer by layer spectra may lead to an intrinsic broadening of the first peak evident in the bulk spectra, due to the relative prominence of this top layer contribution.

Spectroscopy of Li-based Ionic Compounds: **FIG.5(a)** shows the experimental spectra of a series of Li-based ionic compounds, which are of interest for being crucial components of the interphases in batteries as mentioned earlier; namely LiF, LiCl, LiOH, Li_2O, Li_2O_2 and Li_2CO_3. The spectra for the latter three compounds, which were reported in our earlier work[8] exploring the effects of irradiation on Li K-edge spectroscopy, have been included here for the sake of completeness and comparison. It is clear that these Li ionic systems display very different lineshape with features at characteristic energy positions. **FIG.5(b)** shows the theoretical counterparts obtained with MBXAS calculations. Note that these spectra, which are simulated on the static crystal structure at zero temperature, do not incorporate the effects of thermal motion of the ions, which, in addition to smoothening the spectra further, may give rise to new spectral features as a result of local symmetry breaking[20]. In **FIG S2**, we present some of the isovalue plots of the unoccupied orbitals, transitions to which result in the prominent peaks of the spectra according to the MBXAS treatment. For example, in Li_2O_2, the low pre-peak below 58 eV comes from an unoccupied orbital containing predominantly oxygen character hybridized with some contribution from Li-*p* orbital. We can associate this orbital with the low-energy feature reported in O *K*-edge RIXS study of Li_2O_2[33].

sXAS energy Alignment: In the same way that experimental measurements of sXAS require some calibration to align the spectral energies, the simulations performed in this work have their own alignment scheme. However, it is worth noting that the scheme adopted here, as in previous work[20,34,35], relies only on a single experimental spectrum for calibration of all such spectra, defined by the element and the core orbital. Thereafter, all computed spectra should be predictive. This is particularly important when determining the contributions of multiple components to a given spectrum, since their relative alignment can affect the final spectrum, for example, the different peak position of the surface vs. bulk Li atoms of Li metal as detailed above.

In our approach we focus on the particular excited state that we model explicitly at the level of DFT self-consistent-field (SCF) calculations, which is the energetically lowest possible core-excited state for the given element and core orbital. This state has been referred to in the literature as the XCH state (eXcited electron and Core Hole)[36], referring to a neutral reference. XCH is different from the FCH (Full Core Hole) state, which refers to the non-neutral (+1) ionization potential for the core electron. Using relative

XCH total energies, we can align our calculated spectra. The energy range of the spectra themselves are defined by the corresponding KS eigenvalues from the XCH SCF, referenced to the highest occupied orbital from the XCH calculation (which should have the same orbital index as the conduction band minimum or the lowest unoccupied molecular orbital of the ground state). Being familiar with expected underestimation[37,38] of both the electronic band gap and band width by local and semilocal approximations to the exchange-correlation potential in DFT (such as PBE[39]), here we make use of the HSE hybrid exact-exchange functional[40]. For insulators with large band gaps, HSE offers more accurate band structure estimates[41].

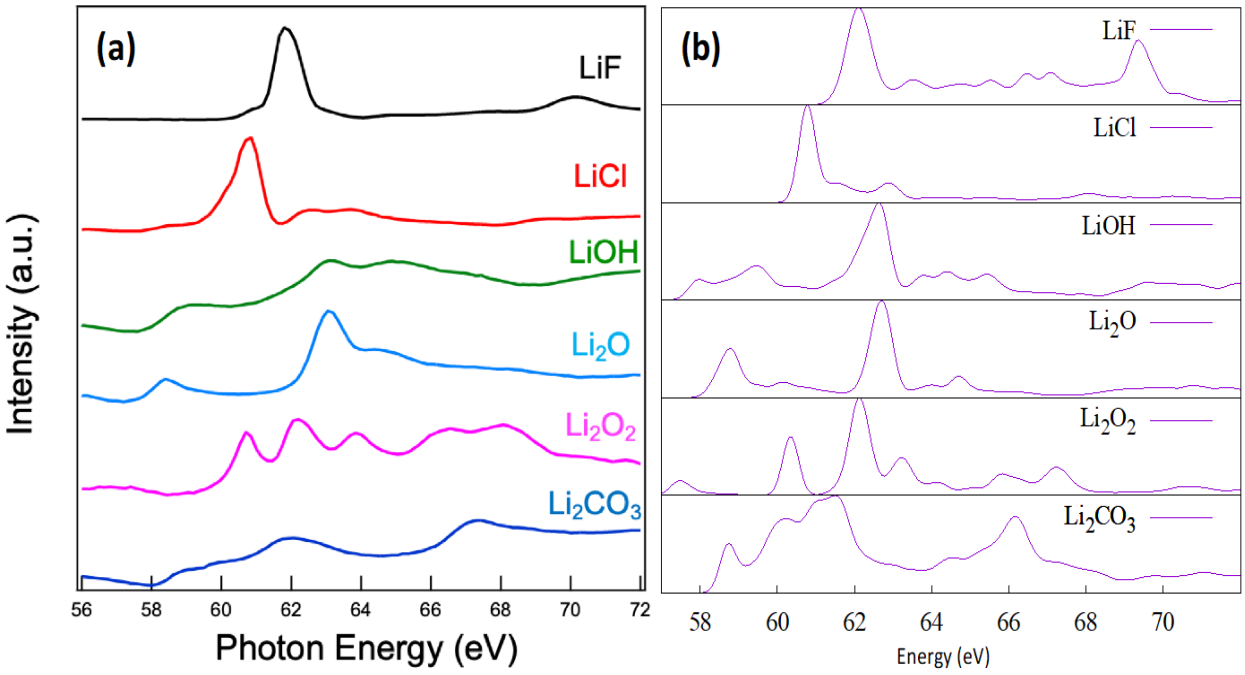

FIG. 5 Panel (a) shows the experimental Li K-edge sXAS spectra of LiF, LiCl, LiOH, Li_2O, Li_2O_2 and Li_2CO_3. Panel (b) shows the theoretical counterparts simulated with MBXAS. A broadening of 0.2 eV has been applied to all of the simulated spectra. For a discussion on the spectral alignment, see main text.

We elucidate the computational scheme with the example of LiF. The lowest possible core-excitation energy can be calculated as $(E_{XCH} - E_{GS})$, where E_{GS} (E_{XCH}) corresponds to the total-energy of the ground state (lowest core-excited state) calculation. However, since these two calculations employ different sets of pseudopotentials, their energies cannot be compared directly and we resort to using a relative excitation energy by referencing the appropriate isolated atom:

$$(E_{XCH} - E_{GS}) - (E_{XCH}^{atom} - E_{GS}^{atom}), \qquad Eq.\ 3$$

where E_{GS}^{atom} (E_{XCH}^{atom}) refers to the energy of a single Li atom in its ground state (lowest core-excited state) obtained with a charge-neutral DFT calculation employing the standard pseudopotential (pseudopotential containing a core-hole). One can think of this relative excitation energy as equivalent to a formation energy difference[34]. In order to guarantee cancellation of systematic errors, the atomic calculations are performed within the same supercell as the full system with the same numerical parameters (plane-wave cut-off, k-point sampling, etc.).

The electronic structure of crystalline LiF exhibits a conduction band minimum with Li $2s$ symmetry. Unsurprisingly, the XCH state places the core-excited electron in a localized orbital with Li $2s$ symmetry centered on the core-excited Li atom. Therefore, the XCH state defines a dark exciton, since $1s \rightarrow 2s$ transitions are dipole-forbidden. The ground state has *N* valence electrons, and so the core-excited states have *N+1* valence electrons. Therefore, the highest occupied orbital of the XCH state has a KS eigenvalue $\tilde{\varepsilon}_{N+1}$. Our calculations indicate that the first bright transition is to the orbital with energy $\tilde{\varepsilon}_{N+3}$. Therefore, the position of the first bright transition in LiF could be approximated as

$$(E_{XCH} - E_{GS}) - (E_{XCH}^{atom} - E_{GS}^{atom}) + (\tilde{\varepsilon}_{N+3} - \tilde{\varepsilon}_{N+1}) + E_{shift}. \qquad Eq.\ 4$$

We apply an analogous expression to align the spectra of each excited atom in all the studied materials, where the orbital index of the first bright transition must be determined in each case. The constant, $E_{shift} = 56.6\ eV$, is added to each spectrum to align it with the experimental photon energy. It was deduced specifically to align the LiF first peak and depends on the specific pseudopotential approximations used (i.e., it is likely not directly transferrable to other calculations which would require their own constant shift). All other energies in Eq. 4 are calculated using the HSE functional. However, the overall spectrum is still computed in its entirety using the PBE functional without any dilation-factor, because the necessary calculations of many unoccupied orbitals is currently too expensive using HSE. There is one exception to this rule: for the spectral alignment of Li metal using Eq.4, the PBE functional is used exclusively, since a local/semi-local functional is better suited for metallic systems in which the properties of the valence electrons are similar to that of the uniform electron gas[42]. Admittedly, this indicates some obvious room for improvement in finding an optimal and transferrable functional and is the subject of future research. As can be seen in **FIG.5(a)** and **FIG.5(b)**, with some quantitative lineshape differences, our calculated spectra show an excellent energy value agreement with the features found in experimental data for all these Li salt compounds tested here.

CONCLUSION

In summary, we have presented a thorough and accurate account of experimental and theoretical investigation of Li *K*-edge sXAS of Li metal and salts. Our experimental findings indicate that, due to the presence of highly reactive Li metal surface even in UHV, a reliable Li-*K* sXAS spectrum of Li metal could only be achieved on fresh *in-situ* cleaved samples in UHV. Additionally, theoretical calculations show that energy resolution will strongly affect the spectral intensity, especially for the first peak, leading to a modified lineshape found in other bulk sensitive techniques compared with the ultra-high-resolution Li-*K* sXAS here. These effects naturally explain the different Li-*K* lineshapes in previous controversial reports. We thus conclude that the intrinsic Li-*K* sXAS spectrum of Li metal features a striking peak at 55.6 eV with a high intensity.

This provides the opportunity to test the different parameters and effects in theoretical calculations. We show that the popular FCH/XCH approach, which expresses the approximate transition probability in terms of the core and the conduction orbital only, is inadequate for reproducing the experimental features. The explicit, many-body response of all the valence electrons to the creation of the core-hole must be taken into account, which we do approximating the true wave function using a Kohn-Sham Slater determinant. Simulations based on room temperature molecular dynamics sampling show that thermal motion of the ions play a crucial role in the smoothening the spectral lineshape. Eventually, we successfully reproduced the experimental results by considering these different effects and contributions from surface atoms, noting the appreciable contributions of non-dipole single-particle transitions to the many-body transition amplitudes in our MBXAS calculations.

In addition to Li metal, we also extended our experimental and theoretical studies to a series of Li-based ionic compounds involved in energy storage materials. We further show the importance of considering total energies as well as KS eigenvalues obtained with hybrid functionals in order to obtain precise relative alignment of the spectra of different materials. This work provides a reliable data bank for Li-*K* spectroscopy of both Li metal and several important salts, as well as developments of theoretical calculations that could reproduce the experimental results at a quantitative level in both the lineshape and energy alignment. The results set a solid benchmark for studying lithium chemistry and reveal critical electronic parameters that define the chemistry of Li compounds.

ASSOCIATED CONTENT

Supporting Information

The Supporting Information file contains a brief account of the determinant based technique used in MBXAS, MBXAS plot of Li K-edge of Li metal using two different values for broadening, Isovalue plot of representative orbitals contributing to the different peaks in the absorption spectra of some of the Li-based compounds, Contribution from different layers in MBXAS of a Li slab, Plot showing standard deviation in the sXAS spectrum of all the Li atoms present in the MD snapshot, plot of X-ray attenuation length as a function of photon energy.

AUTHOR INFORMATION

Corresponding Author

* ychuang@lbl.gov
dgprendergast@lbl.gov
wlyang@lbl.gov

Author Contributions

‡These authors contributed equally.

Funding Sources

All the facilities and efforts are supported by the Office of Science of the US DOE under Contract No. DE-AC02- 05CH11231.

ACKNOWLEDGMENT

Experiments were performed at BL4.0.3 of the Advanced Light Source (ALS), a DOE Office of Science User Facility at the Lawrence Berkeley National Laboratory (LBNL). Theory effort is supported by the LDRD program at the LBNL, and facilitated by a User Program at The Molecular Foundry (TMF). Computational resources were provided by the Lawrencium and the TMF clusters (managed by the High Performance Computing Services Group, at LBNL) and by the National Energy Research Scientific Computing Center (NERSC). W.Y. acknowledges the support from the DOE Data, Artificial Intelligence, and Machine Learning at DOE Scientific User Facilities project. All the facilities and efforts are supported by the Office of Science of the US DOE under Contract No. DE-AC02- 05CH11231. We would like to thank Tod Pascal for helpful discussions and advice.

REFERENCES

(1) Reddy, M. V.; Mauger, A.; Julien, C. M.; Paolella, A.; Zaghib, K. Brief History of Early Lithium-Battery Development. *Materials* 2020, *13* (8), 1884. https://doi.org/10.3390/ma13081884.

(2) Lin, D. Reviving the Lithium Metal Anode for High-Energy Batteries. *NATURE NANOTECHNOLOGY* 2017, *12*, 13.

(3) Krauskopf, T.; Richter, F. H.; Zeier, W. G.; Janek, J. Physicochemical Concepts of the Lithium Metal Anode in Solid-State Batteries. *Chem. Rev.* 2020, *120* (15), 7745–7794. https://doi.org/10.1021/acs.chemrev.0c00431.

(4) Winter, M.; Barnett, B.; Xu, K. Before Li Ion Batteries. *Chem. Rev.* 2018, *118* (23), 11433–11456. https://doi.org/10.1021/acs.chemrev.8b00422.

(5) Xu, K. Electrolytes and Interphases in Li-Ion Batteries and Beyond. *Chem. Rev.* 2014, *114* (23), 11503–11618. https://doi.org/10.1021/cr500003w.

(6) Lin, F.; Liu, Y.; Yu, X.; Cheng, L.; Singer, A.; Shpyrko, O. G.; Xin, H. L.; Tamura, N.; Tian, C.; Weng, T.-C.; Yang, X.-Q.; Meng, Y. S.; Nordlund, D.; Yang, W.; Doeff, M. M. Synchrotron X-Ray Analytical Techniques for Studying Materials Electrochemistry in Rechargeable Batteries. *Chem. Rev.* 2017, *117* (21), 13123–13186. https://doi.org/10.1021/acs.chemrev.7b00007.

(7) B.L. Henke, E.M. Gullikson, J.C. David. X-Ray Interactions: Photoabsorption, Scattering, Transmission, and Reflection at E=50-30000 EV, Z=1-92, Atomic Data and Nuclear Data Tables. 1993, *54* (2), 181–342.

(8) Qiao, R.; Chuang, Y.-D.; Yan, S.; Yang, W. Soft X-Ray Irradiation Effects of Li2O2, Li2CO3 and Li2O Revealed by Absorption Spectroscopy. *PLoS ONE* 2012, *7* (11), e49182. https://doi.org/10.1371/journal.pone.0049182.

(9) Braun, A.; Wang, H.; Shim, J.; Lee, S. S.; Cairns, E. J. Lithium K(1s) Synchrotron NEXAFS Spectra of Lithium-Ion Battery Cathode, Anode and Electrolyte Materials. *Journal of Power Sources* 2007, *170* (1), 173–178. https://doi.org/10.1016/j.jpowsour.2007.04.022.

(10) Wang, D.; Zuin, L. Li K-Edge X-Ray Absorption near Edge Structure Spectra for a Library of Lithium Compounds Applied in Lithium Batteries. *Journal of Power Sources* 2017, *337*, 100–109. https://doi.org/10.1016/j.jpowsour.2016.10.105.

(11) Tsuji, J.; Nakamatsu, H.; Mukoyama, T.; Kojima, K.; Ikeda, S.; Taniguchi, K. Lithium K-Edge XANES Spectra for Lithium Compounds. *X-Ray Spectrom.* 2002, *31* (4), 319–326. https://doi.org/10.1002/xrs.577.

(12) Yogi, C.; Takamatsu, D.; Yamanaka, K.; Arai, H.; Uchimoto, Y.; Kojima, K.; Watanabe, I.; Ohta, T.; Ogumi, Z. Soft X-Ray Absorption Spectroscopic Studies with Different Probing Depths: Effect of an Electrolyte Additive on Electrode Surfaces. *Journal of Power Sources* 2014, *248*, 994–999. https://doi.org/10.1016/j.jpowsour.2013.10.030.

(13) Mizota, H.; Ito, Y.; Tochio, T.; Handa, K.; Takekawa, S.; Kitamura, K. Li K-Edge XANES Spectra of Lithium Niobate and Lithium Tantalite. In *AIP Conference Proceedings*; AIP: Stanford, California (USA), 2007; Vol. 882, pp 508–510. https://doi.org/10.1063/1.2644575.

(14) O'Shaughnessy, C.; Henderson, G. S.; Moulton, B. J. A.; Zuin, L.; Neuville, D. R. A Li *K*-Edge XANES Study of Salts and Minerals. *J Synchrotron Rad* 2018, *25* (2), 543–551. https://doi.org/10.1107/S1600577518000954.

(15) Orikasa, Y.; Furutani, J.; Yamanaka, K.; Ohta, T. Lithium K-Edge X-Ray Absorption Analysis of Lithium-Ion Battery Cathodes. 2019, No. 21, 4.

(16) Zhuo, Z.; Dai, K.; Qiao, R.; Wang, R.; Wu, J.; Liu, Y.; Peng, J.; Chen, L.; Chuang, Y.; Pan, F.; Shen, Z.; Liu, G.; Li, H.; Devereaux, T. P.; Yang, W. Cycling Mechanism of Li2MnO3: Li–CO2 Batteries and Commonality on Oxygen Redox in Cathode Materials. *Joule* 2021, S2542435121000817. https://doi.org/10.1016/j.joule.2021.02.004.

(17) Haensel, R.; Keitel, G.; Sonntag, B.; Kunz, C.; Schreiber, P. Photoabsorption Measurement of Li, Be, Na, Mg, and Al in the XUV Range. *Phys. Stat. Sol. (a)* 1970, *2* (1), 85–90. https://doi.org/10.1002/pssa.19700020110.

(18) Hightower, A.; Ahn, C. C.; Fultz, B.; Rez, P. Electron Energy-Loss Spectrometry on Lithiated Graphite. *Appl. Phys. Lett.* 2000, *77* (2), 238–240. https://doi.org/10.1063/1.126936.

(19) Schülke, W.; Nagasawa, H.; Mourikis, S.; Lanzki, P. Dynamic Structure of Electrons in Li Metal: Inelastic Synchrotron x-Ray Scattering Results and Interpretation beyond the Random-Phase Approximation. *Phys. Rev. B* 1986, *33* (10), 6744–6757. https://doi.org/10.1103/PhysRevB.33.6744.

(20) Pascal, T. A.; Boesenberg, U.; Kostecki, R.; Richardson, T. J.; Weng, T.-C.; Sokaras, D.; Nordlund, D.; McDermott, E.; Moewes, A.; Cabana, J.; Prendergast, D. Finite Temperature Effects on the X-Ray Absorption Spectra of Lithium Compounds: First-Principles Interpretation of X-Ray Raman Measurements. *The Journal of Chemical Physics* 2014, *140* (3), 034107. https://doi.org/10.1063/1.4856835.

(21) Fister, T. T.; Schmidt, M.; Fenter, P.; Johnson, C. S.; Slater, M. D.; Chan, M. K. Y.; Shirley, E. L. Electronic Structure of Lithium Battery Interphase Compounds: Comparison between Inelastic x-Ray Scattering Measurements and Theory. *The Journal of Chemical Physics* 2011, *135* (22), 224513. https://doi.org/10.1063/1.3664620.

(22) Hohenberg, P.; Kohn, W. Inhomogeneous Electron Gas. *Phys. Rev.* 1964, *136* (3B), B864–B871. https://doi.org/10.1103/PhysRev.136.B864.

(23) Kohn, W.; Sham, L. J. Self-Consistent Equations Including Exchange and Correlation Effects. *Phys. Rev.* 1965, *140* (4A), A1133–A1138. https://doi.org/10.1103/PhysRev.140.A1133.

(24) Shirley, E. L. *Ab Initio* Inclusion of Electron-Hole Attraction: Application to X-Ray Absorption and Resonant Inelastic X-Ray Scattering. *Phys. Rev. Lett.* 1998, *80* (4), 794–797. https://doi.org/10.1103/PhysRevLett.80.794.

(25) Rohlfing, M.; Louie, S. G. Electron-Hole Excitations and Optical Spectra from First Principles. *Phys. Rev. B* 2000, *62* (8), 4927–4944. https://doi.org/10.1103/PhysRevB.62.4927.

(26) Mauchamp, V.; Boucher, F.; Ouvrard, G.; Moreau, P. *Ab Initio* Simulation of the Electron Energy-Loss near-Edge Structures at the Li K Edge in Li, Li 2 O , and Li Mn 2 O 4. *Phys. Rev. B* 2006, *74* (11), 115106. https://doi.org/10.1103/PhysRevB.74.115106.

(27) Liang, Y.; Vinson, J.; Pemmaraju, S.; Drisdell, W. S.; Shirley, E. L.; Prendergast, D. Accurate X-Ray Spectral Predictions: An Advanced Self-Consistent-Field Approach Inspired by Many-Body Perturbation Theory. *Phys. Rev. Lett.* 2017, *118* (9), 096402. https://doi.org/10.1103/PhysRevLett.118.096402.

(28) Liang, Y.; Prendergast, D. Quantum Many-Body Effects in x-Ray Spectra Efficiently Computed Using a Basic Graph Algorithm. *Phys. Rev. B* 2018, *97* (20), 205127. https://doi.org/10.1103/PhysRevB.97.205127.

(29) Liang, Y.; Prendergast, D. Taming Convergence in the Determinant Approach for X-Ray Excitation Spectra. *Phys. Rev. B* 2019, *100* (7), 075121. https://doi.org/10.1103/PhysRevB.100.075121.

(30) Storr, J. *NEXAFS Spectroscopy*; Springer Series in Surface Sciences; Springer-Verlag Berlin Heidelberg, 1992; Vol. 25.

(31) Yang, W. L. Band Structure and Fermi Surface of Electron-Doped C60 Monolayers. *Science* 2003, *300* (5617), 303–307. https://doi.org/10.1126/science.1082174.

(32) Krisch, M. H.; Sette, F.; Masciovecchio, C.; Verbeni, R. Momentum Transfer Dependence of Inelastic X-Ray Scattering from the Li K Edge. *Phys. Rev. Lett.* 1997, *78* (14), 2843–2846. https://doi.org/10.1103/PhysRevLett.78.2843.

(33) Zhuo, Z.; Pemmaraju, C. D.; Vinson, J.; Jia, C.; Moritz, B.; Lee, I.; Sallies, S.; Li, Q.; Wu, J.; Dai, K.; Chuang, Y.; Hussain, Z.; Pan, F.; Devereaux, T. P.; Yang, W. Spectroscopic Signature of Oxidized Oxygen States in Peroxides. *J. Phys. Chem. Lett.* 2018, *9* (21), 6378–6384. https://doi.org/10.1021/acs.jpclett.8b02757.

(34) Jiang, P.; Prendergast, D.; Borondics, F.; Porsgaard, S.; Giovanetti, L.; Pach, E.; Newberg, J.; Bluhm, H.; Besenbacher, F.; Salmeron, M. Experimental and Theoretical Investigation of the Electronic Structure of Cu_2O and CuO Thin Films on Cu(110) Using x-Ray Photoelectron and Absorption Spectroscopy. *The Journal of Chemical Physics* 2013, *138* (2), 024704. https://doi.org/10.1063/1.4773583.

(35) England, A. H.; Duffin, A. M.; Schwartz, C. P.; Uejio, J. S.; Prendergast, D.; Saykally, R. J. On the Hydration and Hydrolysis of Carbon Dioxide. *Chemical Physics Letters* 2011, *514* (4–6), 187–195. https://doi.org/10.1016/j.cplett.2011.08.063.
(36) Prendergast, D.; Galli, G. X-Ray Absorption Spectra of Water from First Principles Calculations. *Phys. Rev. Lett.* 2006, *96* (21), 215502. https://doi.org/10.1103/PhysRevLett.96.215502.
(37) Mori-Sánchez, P.; Cohen, A. J.; Yang, W. Localization and Delocalization Errors in Density Functional Theory and Implications for Band-Gap Prediction. *Phys. Rev. Lett.* 2008, *100* (14), 146401. https://doi.org/10.1103/PhysRevLett.100.146401.
(38) Perdew, J. P.; Yang, W.; Burke, K.; Yang, Z.; Gross, E. K. U.; Scheffler, M.; Scuseria, G. E.; Henderson, T. M.; Zhang, I. Y.; Ruzsinszky, A.; Peng, H.; Sun, J.; Trushin, E.; Görling, A. Understanding Band Gaps of Solids in Generalized Kohn–Sham Theory. *Proc Natl Acad Sci USA* 2017, *114* (11), 2801–2806. https://doi.org/10.1073/pnas.1621352114.
(39) Perdew, J. P.; Burke, K.; Ernzerhof, M. Generalized Gradient Approximation Made Simple. *Phys. Rev. Lett.* 1996, *77* (18), 3865–3868. https://doi.org/10.1103/PhysRevLett.77.3865.
(40) Heyd, J.; Scuseria, G. E.; Ernzerhof, M. Hybrid Functionals Based on a Screened Coulomb Potential. *The Journal of Chemical Physics* 2003, *118* (18), 8207–8215. https://doi.org/10.1063/1.1564060.
(41) Heyd, J.; Scuseria, G. E. Efficient Hybrid Density Functional Calculations in Solids: Assessment of the Heyd–Scuseria–Ernzerhof Screened Coulomb Hybrid Functional. *The Journal of Chemical Physics* 2004, *121* (3), 1187–1192. https://doi.org/10.1063/1.1760074.
(42) Janesko, B. G.; Henderson, T. M.; Scuseria, G. E. Screened Hybrid Density Functionals for Solid-State Chemistry and Physics. *Phys. Chem. Chem. Phys.* 2009, *11* (3), 443–454. https://doi.org/10.1039/B812838C.

SUPPLEMENTARY INFORMATION

Controlled experiments and optimized theory of absorption spectra of Li metal and salts

Subhayan Roychoudhury§#†, Zengqing Zhuo§†, Ruimin Qiao§†, Liwen Wan¶, Yufeng Liang#, Feng Pan‡, Yi-de Chuang§*, David Prendergast#* and Wanli Yang§*

§Advanced Light Source, Lawrence Berkeley National Laboratory, 1 Cyclotron Road, Berkeley CA 94720, USA
¶Lawrence Livermore National Laboratory, 7000 East Avenue, Livermore, California 94550, USA
‡School of Advanced Materials, Peking University Shenzhen Graduate School, Shenzhen 518055, China
#The Molecular Foundry, Lawrence Berkeley National Laboratory, 1 Cyclotron Road, Berkeley CA 94720, USA

Determinant based technique used in MBXAS

Simulations of Li K-edge spectra are performed with the MBXAS approach[1–3], which uses the energy and Kohn-Sham orbitals calculated with the plane-wave DFT code, pw.x, within the QuantumESPRESSO suite[4]. Since a core-excited state calculation involves an atom containing one less core electron (represented by the appropriate pseudopotential), electronic structure calculations were performed with large supercells to minimize the effects of interaction among the periodic replicas. Bulk Li simulations were performed with a cubic supercell of length ~26 a.u. For simulation of the (100) Li slab, a vacuum of ~36 a.u. is added above the surface layer. DFT calculations were performed employing ultrasoft pseudopotentials and a plane-wave kinetic energy cutoff of 25 Ry (200Ry) was used to represent the wave functions (elecron density). All calculations on Li metal (bulk and slab) have been performed with the $f^{(2)}$approximation (including one additional valence electron-hole pair besides the core-hole and excited electron), which is adequate for convergence[3], while those on the compounds have been performed with the $f^{(1)}$ approximation (just include the core-hole and excited electron). In a calculation denoted $f^{(M)}$, the code can create up to (*M-1*) electron-hole pairs in the valence subspace in addition to the core-excitation. Typically, a calculation with M > 1 is deemed necessary only for metals and small-gap semiconductors because of the low energy required to create an additional valence excitation.

In MBXAS, the transition matrix elements are expressed as:

$$\langle \Psi_{\mathrm{f}} | \hat{\mathbf{O}} | \Psi_{\mathrm{i}} \rangle = \sum_{c}^{empty} \langle \Psi_{\mathrm{f}} | \Psi_i^c \rangle \langle \phi_c | \hat{\mathbf{o}} | \phi_{\mathrm{core}} \rangle$$

Where $\langle \Psi_{\mathrm{f}} | \Psi_i^c \rangle$ follows the relation

$$\langle \Psi_{\mathrm{f}} | \Psi_i^c \rangle^* = \det \begin{bmatrix} \xi_{\tilde{f}_1,1} & \xi_{\tilde{f}_1,2} & \cdots & \xi_{\tilde{f}_1,N} & \xi_{\tilde{f}_1,c} \\ \vdots & \vdots & \ddots & \vdots & \vdots \\ \xi_{\tilde{f}_{N+1},1} & \xi_{\tilde{f}_{N+1},2} & \cdots & \xi_{\tilde{f}_{N+1},N} & \xi_{\tilde{f}_{N+1},c} \end{bmatrix}.$$

Here, $\{\tilde{f}_1, \tilde{f}_2, \cdots, \tilde{f}_{N+1}\}$ is the electron configuration of final-state orbitals (obtained with an SCF calculation employing the core-hole pseudopotential) constituting Ψ_{f} and $\xi_{\tilde{f}_l,m} = \langle \phi_m | \widetilde{\phi_{\tilde{f}_l}} \rangle$, where a ~ on top denotes a final state orbital index. FIG 4C in the main text shows, within a certain range encompassing the highest occupied level, the heat-map of the absolute values of the elements of the matrix ξ.

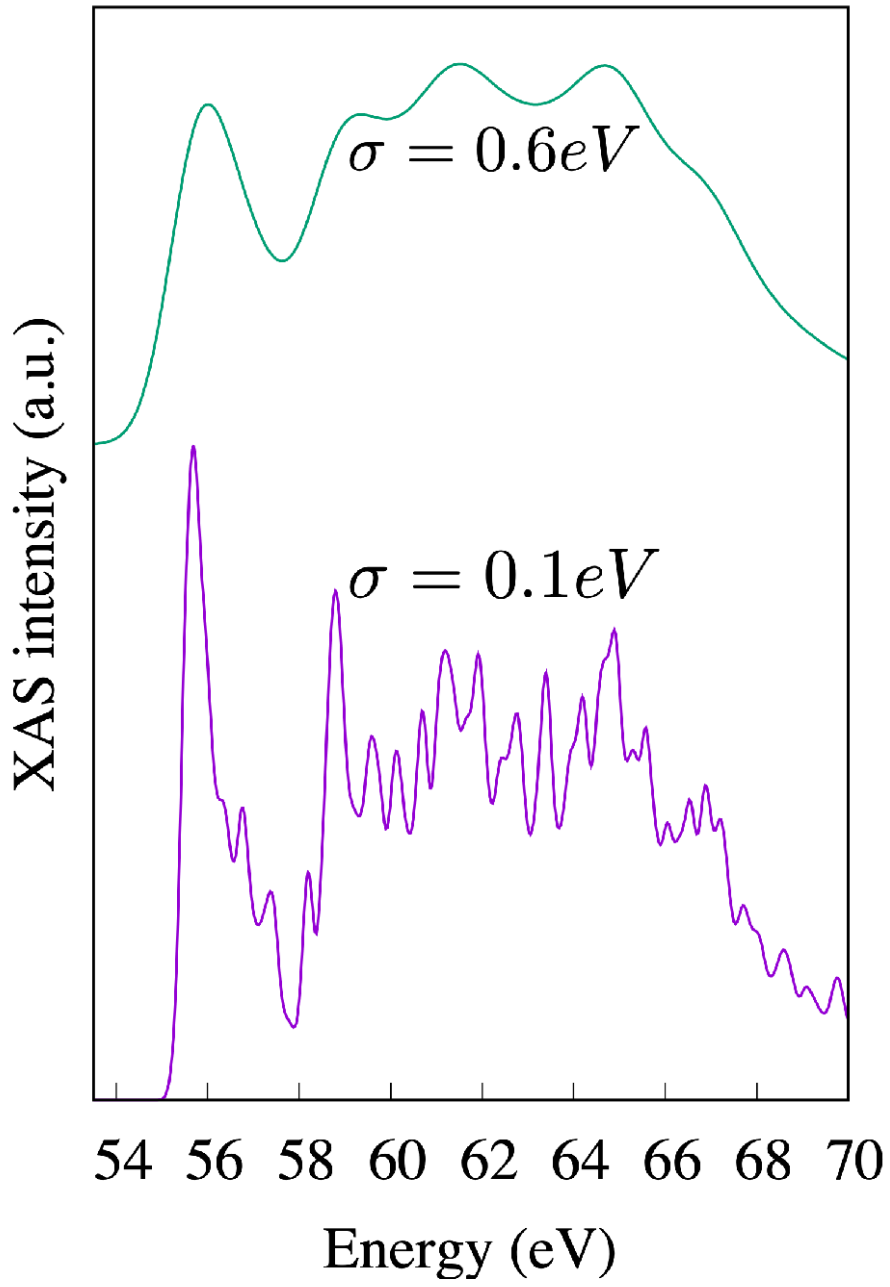

FIG S1: MBXAS plot of Li K-edge sXAS of pristine bulk Li for two different values of numerical broadening, 0.1 eV and 0.6 eV.

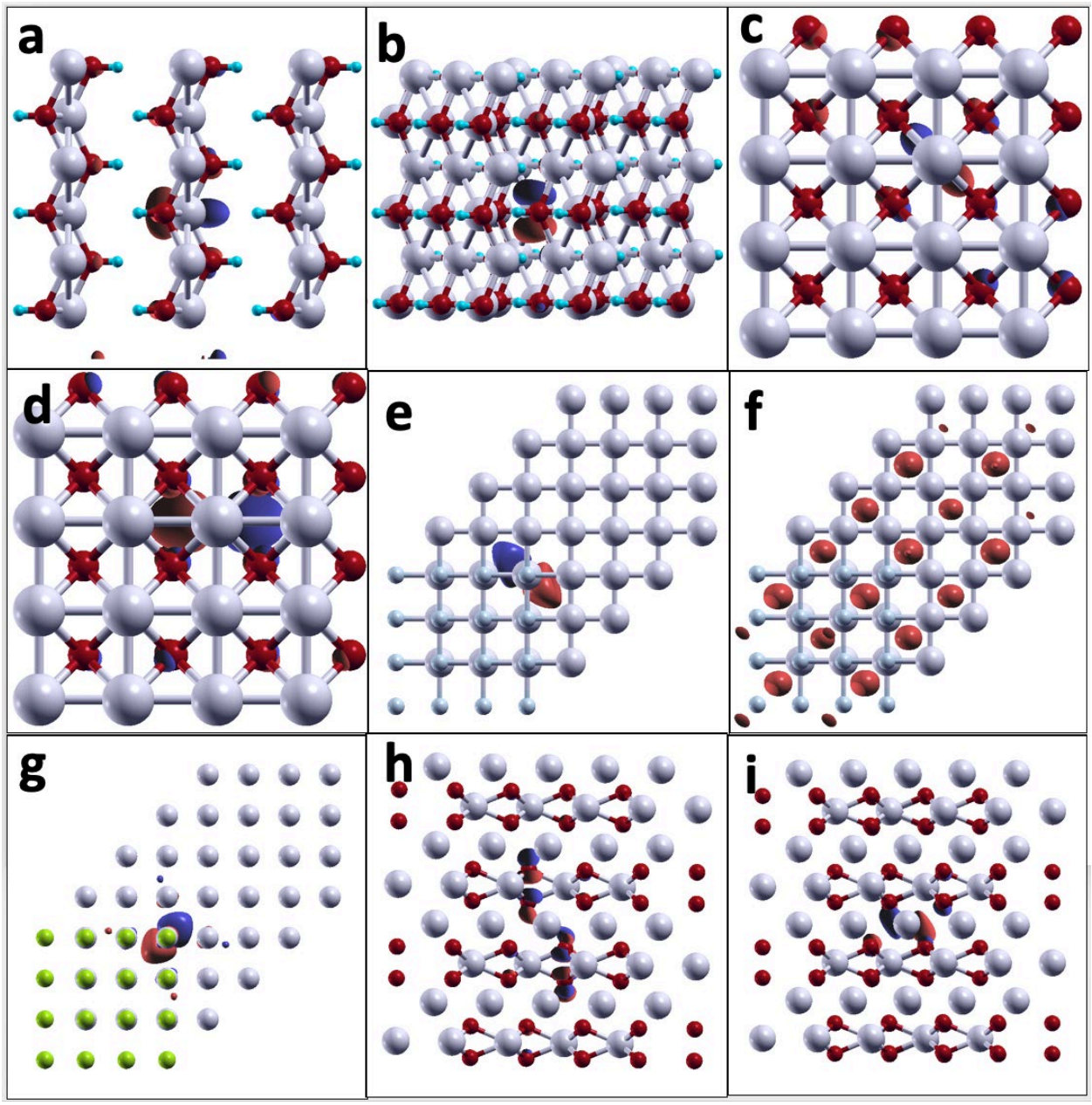

FIG S2: Isovalue plot of representative orbitals contributing to the different peaks in the absorption spectra of some of the Li-based compounds. (a) Peak at ~59.5 eV for LiOH, (b) peak at ~61.6 eV for LiOH, (c) peak at ~58.8 eV for Li_2O, (d) peak at ~62.7 eV for Li_2O, (e) peak at ~62.1 eV for LiF, (f) peak at ~69.4 eV for LiF, (g) peak at ~60.8 eV for LiCl, (h) pre-peak at ~57.5 eV for Li_2O_2 , (i) intense peak at ~62.1 eV for Li_2O_2 .

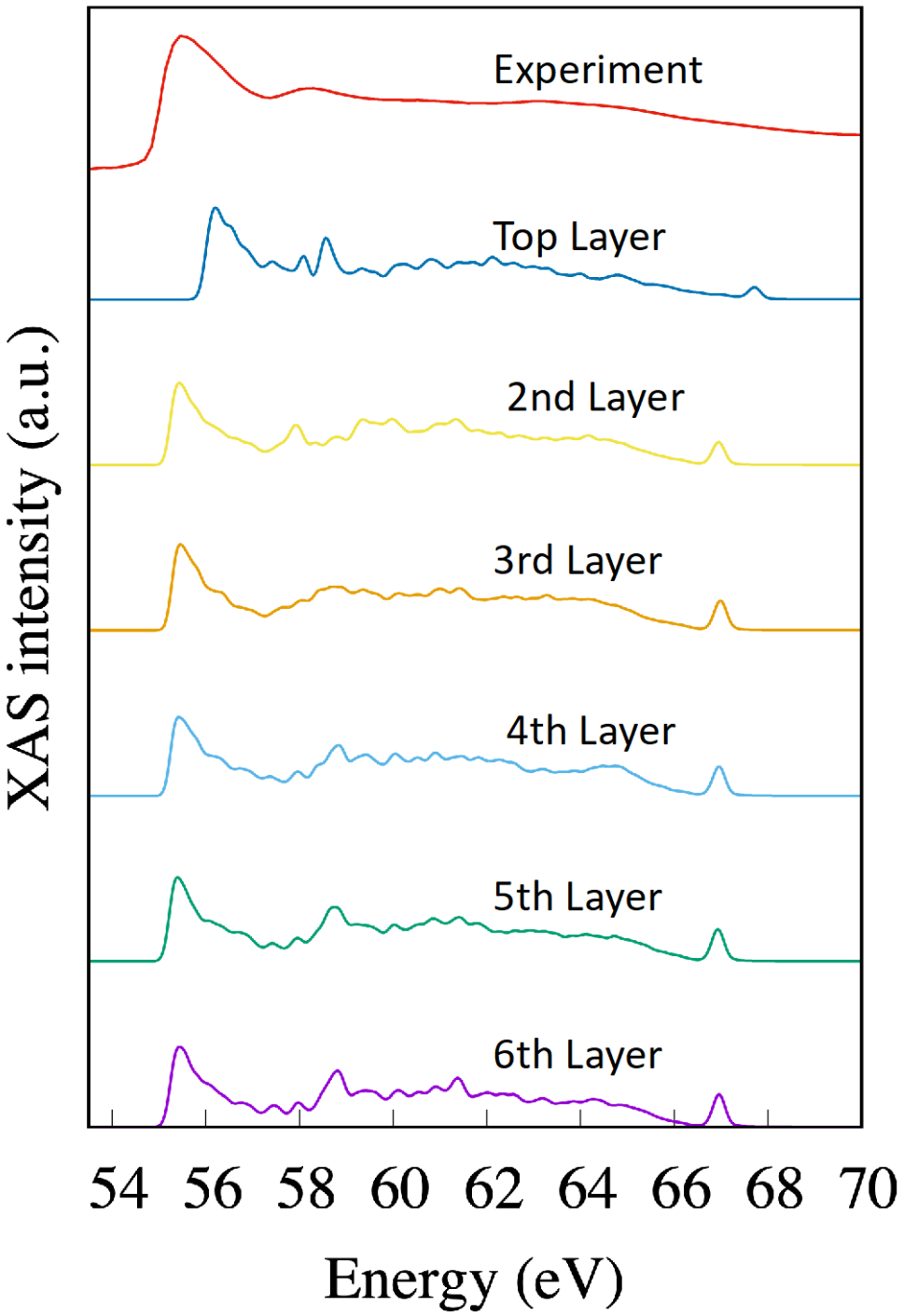

FIG S3: Simulated sXAS plots of the top (blue), 2nd (yellow), 3rd (orange), 4th (indigo), 5th (green) and 6th (violet) layers of the 12-layer thick Li slab. The experimental plot (red) is presented on top. This plot shows that the layer-by-layer spectrum of the slab converges within the first 4 layers and therefore, the experimental spectrum, which corresponds to an attenuation length of tens of nanometers, essentially probes the bulk electronic structure.

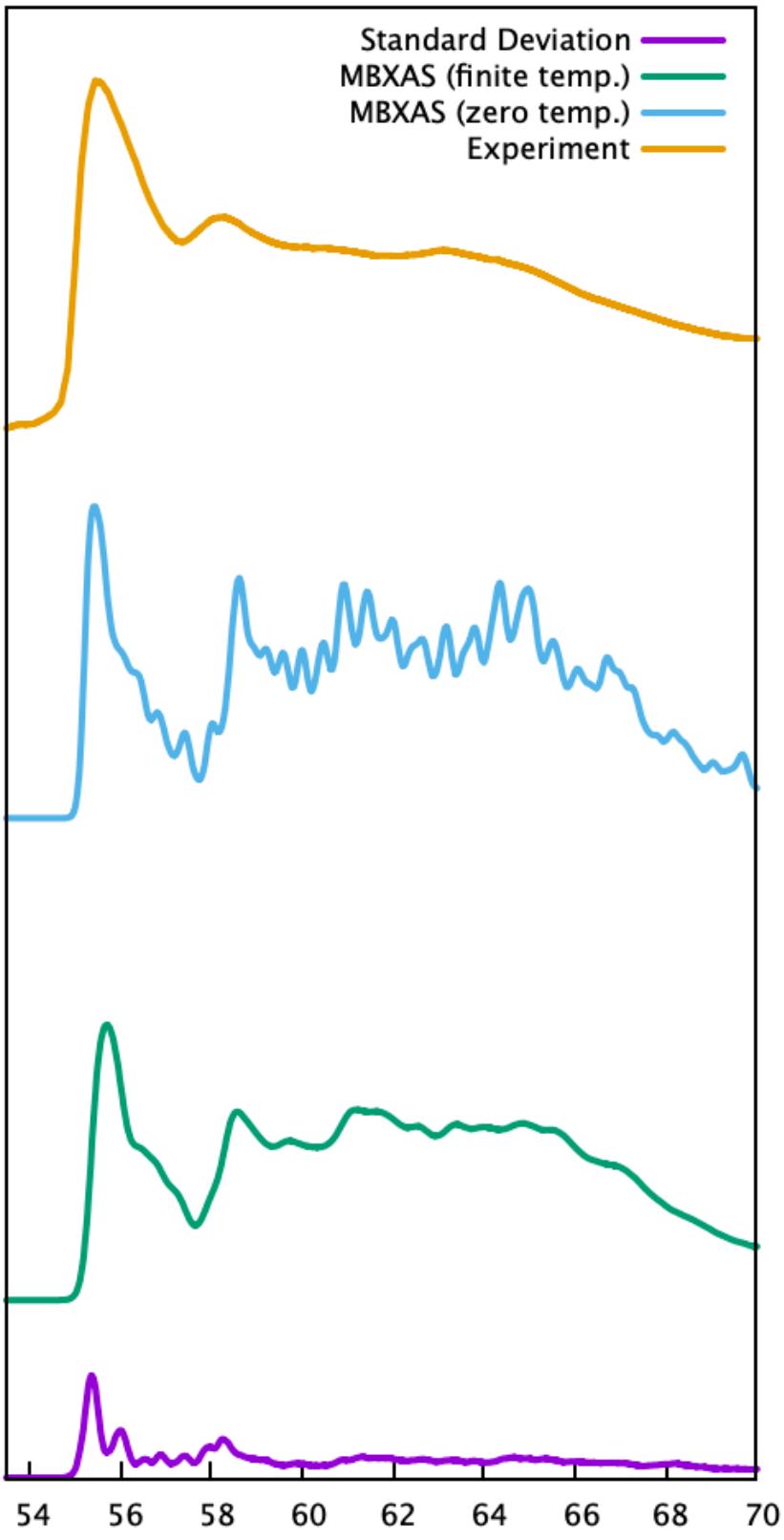

FIG S4: Experimental Li K-edge spectrum (top), MBXAS plot of the static crystal at zero temperature (2nd from top), MBXAS plot calculated from a snapshot obtained using room-

temperature MD with a 128 atom Li crystal (3rd from top). The bottommost plot shows the standard deviation (SD) of the spectra of all the atoms present in the MD snapshot. (The top 3 plots are shown in Fig 3 in the main text. They are re-presented here to facilitate comparison with the SD plot).

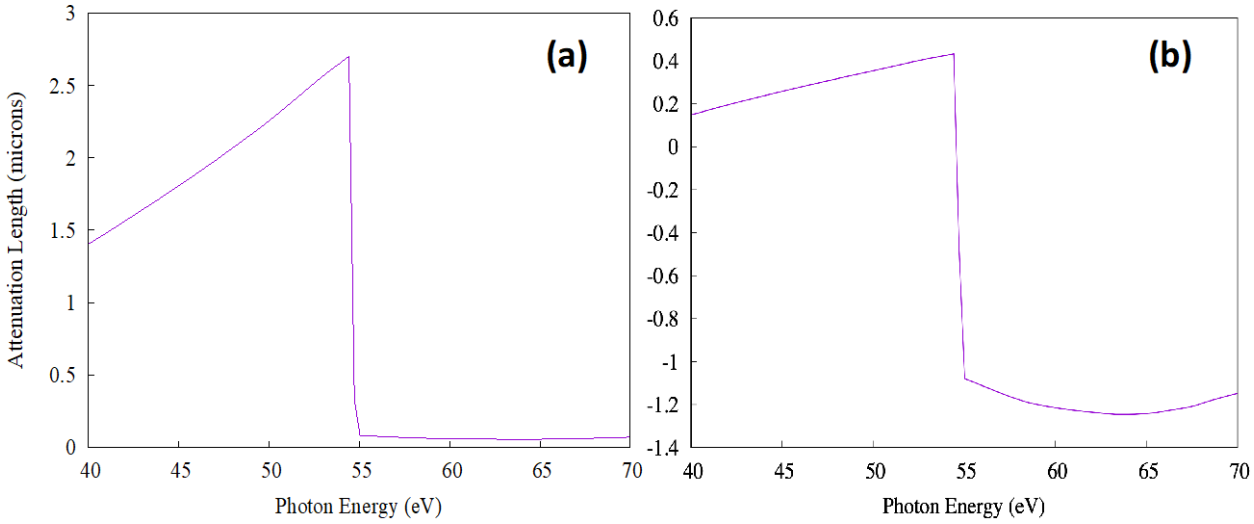

FIG S5: Plot of X-ray attenuation length as a function of photon energy incident normal to the Li metal surface. Panel (a) and (b) shows the attenuation in the standard (micron) scale and in $\log_{10}$ scale, respectively. The data for this plot is obtained from (https://henke.lbl.gov/optical_constants)[5]

(1) Liang, Y.; Vinson, J.; Pemmaraju, S.; Drisdell, W. S.; Shirley, E. L.; Prendergast, D. Accurate X-Ray Spectral Predictions: An Advanced Self-Consistent-Field Approach Inspired by Many-Body Perturbation Theory. *Phys. Rev. Lett.* **2017**, *118* (9), 096402. https://doi.org/10.1103/PhysRevLett.118.096402.

(2) Liang, Y.; Prendergast, D. Quantum Many-Body Effects in x-Ray Spectra Efficiently Computed Using a Basic Graph Algorithm. *Phys. Rev. B* **2018**, *97* (20), 205127. https://doi.org/10.1103/PhysRevB.97.205127.

(3) Liang, Y.; Prendergast, D. Taming Convergence in the Determinant Approach for X-Ray Excitation Spectra. *Phys. Rev. B* **2019**, *100* (7), 075121. https://doi.org/10.1103/PhysRevB.100.075121.

(4) Giannozzi, P.; Baroni, S.; Bonini, N.; Calandra, M.; Car, R.; Cavazzoni, C.; Ceresoli, D.; Chiarotti, G. L.; Cococcioni, M.; Dabo, I.; Dal Corso, A.; de Gironcoli, S.; Fabris, S.; Fratesi, G.; Gebauer, R.; Gerstmann, U.; Gougoussis, C.; Kokalj, A.; Lazzeri, M.; Martin-Samos, L.; Marzari, N.; Mauri, F.; Mazzarello, R.; Paolini, S.; Pasquarello, A.; Paulatto, L.;

Sbraccia, C.; Scandolo, S.; Sclauzero, G.; Seitsonen, A. P.; Smogunov, A.; Umari, P.; Wentzcovitch, R. M. QUANTUM ESPRESSO: A Modular and Open-Source Software Project for Quantum Simulations of Materials. *J. Phys.: Condens. Matter* **2009**, *21* (39), 395502. https://doi.org/10.1088/0953-8984/21/39/395502.

(5) B.L. Henke, E.M. Gullikson, J.C. David. X-Ray Interactions: Photoabsorption, Scattering, Transmission, and Reflection at E=50-30000 EV, Z=1-92, Atomic Data and Nuclear Data Tables. **1993**, *54* (2), 181–342.